PAPER

Check for updates

Tuneable CO_2 binding enthalpies by redox modulation of an electroactive MOF-74 framework†

Patrick W. Doheny,[a] Ravichandar Babarao, [ID][b] Cameron J. Kepert*[a] and Deanna M. D'Alessandro [ID] *[a]

The [M_2(dobdc)] series of frameworks (also known as MOF-74 and CPO-27, where M^{2+} = Zn, Mg, for example, and dobdc^{2-} = 4,6-dioxido-1,3-benzenedicarboxylate) have been the subject of enormous interest in respect to their attractive gas adsorption properties that arise from the ultra-high concentration of open metal sites. An interesting prospect with respect to future applications of these materials is the possibility of generating a 'switchable' framework in which the guest adsorption can be modulated by virtue of the redox state of the framework. Herein, we report a closely related metal–organic framework (MOF), [Zn_2(DSNDI)], where the redox state of the electroactive ligand DSNDI^{4-} (N,N'-bis(4-carboxy-3-hydroxyphenyl)-1,4,5,8-naphthalenetetracarboxydiimide) can be modulated using both *in situ* and *ex situ* methods. The material is stable to both chemical and electrochemical reduction of its organic DSNDI units without structural collapse or degradation, and remains porous to N_2, H_2 and CO_2. The chemically reduced frameworks demonstrate notable changes from the parent material, particularly with respect to CO_2 binding. The CO_2 isosteric heat of adsorption (Q_{st}) increases from 27.9 kJ mol^{-1} in the neutral material to 43.9 kJ mol^{-1} after reduction due to enhanced host–guest interactions, the latter being comparable to the best performing member of the MOF-74 series, [Mg_2(dobdc)]. The origin of the enhanced interaction was probed using Density Functional Theory (DFT) calculations which corroborated the presence of enhanced framework-CO_2 interactions for the chemically-reduced MOF. The tuneable CO_2 binding character provides an attractive mechanism to tune gas separations and capture.

Introduction

Metal–organic framework (MOF) materials have long been recognised as promising candidates for a wide range of applications including, but not limited to, CO_2 storage,[1–3] separations[4–7] and electrocatalysis.[8–11] In the field of gas sorption,[12–14] storage and crude separations,[7,15–17] the MOF-74/CPO-27 material,[12] ([M_2(dobdc)], where M^{2+} = Mg, Mn, Fe, Co, Ni, Cu and Zn and dobdc^{2-} = 4,6-dioxido-1,3-benzenedicarboxylate), enjoys significant attention due to its porosity and ultra-high concentration of open metal sites that facilitate relatively strong guest binding compared with typical physisorption in framework materials.[18]

One attractive means by which multifunctional properties within a MOF may coexist or be tuned (such as gas sorption or selectivity) is by use of a redox 'switch', where certain characteristics emerge as a result of oxidation or reduction.[19–22] Despite this, the study of electroactive MOF-74 materials is comparatively limited and mostly confined to redox-transformations of the metal ions such as $Fe^{2+/3+}$ oxidation.[23] Post-synthetic oxidation of the dobdc^{2-} ligand has also been reported,[24] in addition to the use of 2,5-disulfhydrylbenzene-1,4-dicarboxylate which led to an enhanced charge mobility relative to the [M_2(dobdc)] material.[25]

A recent report by Saha[26] described the synthesis of a MOF-74 analogue incorporating the redox-active DSNDI ligand (where DSNDI^{4-} = N,N'-bis(4-carboxy-3-hydroxyphenyl)-1,4,5,8-naphthalenetetracarboxydiimide) in which the band gap of the framework was modified by infiltrating tetrathiafulvalene (TTF) electron donors that interacted with the DSNDI acceptor units. An additional report by Dincă[27] focused on an analogous framework utilising a regioisomer of the DSNDI ligand, NDISA

[a] *School of Chemistry, The University of Sydney, New South Wales, 2006, Australia.*
E-mail: deanna.dalessandro@sydney.edu.au, cameron.kepert@sydney.edu.au;
Tel: +61 2 93513777

[b] *School of Science, Royal Melbourne Institute of Technology (RMIT University),*
Victoria, 3001, Australia.

(where NDISA^{4-} = N,N'-bis(3-carboxy-4-hydroxyphenyl)-1,4,5,8-naphthalenetetradicarboximide) that was studied for electrochromic applications upon *in situ* reduction of the ligand.

Motivated by previous work suggesting that the gas sorption properties of MOFs can be switched by redox modulation,[28–30] we now report the electroactive properties of the [Zn$_2$(DSNDI)] framework, hereafter denoted **1**, *via* a combination of *in situ* and *ex situ* techniques. Particular attention was focused on the modification of its gas sorption properties (N$_2$, H$_2$, CH$_4$ and CO$_2$), and the CO$_2$ binding enthalpies by utilising post-synthetic chemical reduction. Density Functional Theory (DFT) calculations were employed to gain insights into the origins of the enhanced framework-CO$_2$ interactions for the chemically-reduced materials. Such studies are important given the strong attention that the parent MOF-74 materials have received with respect to their guest sorption properties. Notably, the presence of 1D honeycomb pores and an ultra-high concentration of open metal binding sites upon activation of the materials makes them highly attractive for industrial gas capture and separations applications. The realisation of tuneable guest adsorption by virtue of a redox-active ligand enhances the multifunctionality of this family of frameworks.

Results and discussion

Electrochemical and spectroelectrochemical properties

The electrochemical properties of **1** were examined using cyclic voltammetry (CV) in 0.1 M [(n-C$_4$H$_9$)$_4$N]PF$_6$/DMF supporting electrolyte. The CV (Fig. 1) showed two processes in the cathodic region with a reversible, first process at −0.89 V *vs.* Fc/Fc$^+$ and a second, *quasi*-reversible process at −1.41 V *vs.* Fc/Fc$^+$ that became increasingly reversible at faster scan rates consistent with the electrochemistry of previously reported naphthalenediimide (NDI) containing frameworks.[31] Given

Fig. 1 CV of **1** in 0.1 M [(n-C$_4$H$_9$)$_4$N]PF$_6$/DMF supporting electrolyte at scan rates of 25–250 mV s^{-1}. The arrow indicates the direction of the forward scan.

the redox-innocent nature of the Zn^{2+} nodes of the framework, the observed processes were assigned to the sequential electrochemical reduction of the NDI moiety of the DSNDI ligands within the MOF structure to the NDI radical anion and subsequent dianion species.[27,28,32] This was supported by solution-state CV of the DSNDI ligand (Fig. S2, ESI†) which correlated well with that of the framework, showing that the redox properties of the ligand had been successfully transferred to the MOF.

The optical properties of the neutral and reduced species of **1** were examined using *in situ* solid-state UV-Vis-NIR spectroelectrochemistry in 0.1 M [(n-C$_4$H$_9$)$_4$N]PF$_6$/DMF supporting electrolyte. The diffuse reflectance spectrum of the neutral material at 0 V (Fig. 2a) was characterised by a single band at 23 510 cm^{-1} that was attributed to the aromatic $\pi \rightarrow \pi^*$ transition of the DSNDI ligand. Upon reduction at −1.2 V, bands in the visible region formed at 12 810, 14 260 and 16 520 cm^{-1} in addition to a sharp band at 21 050 cm^{-1}; these were attributed to the formation of the DSNDI radical anion within the framework structure.[33,34] The emergence of the new bands was concurrent with a colour change of the initially bright orange material to a deep brown and correlates well with the spectroelectrochemistry of the H$_4$DSNDI ligand (Fig. S3 and S4, ESI†). Changing the potential further to −2.0 V (Fig. 2b) led to the sample turning black with a large increase in the spectral intensity alongside the appearance of bands at 17 150, 18 010, 19 010 and 19 940 cm^{-1} consistent with the formation of a dianionic NDI species.[33,34]

Returning the potential to 0 V (Fig. S5, ESI†) led to the slow decay of the visible bands and restoration of the initial spectrum over the course of several hours. The slow decay of the radical bands after the removal of the applied potential implied the formation of a stable anionic radical. The restoration of the initial spectrum and sample colour upon returning the potential to 0 V was suggestive of a degree of reversibility and stability of **1** to electrochemical reduction.

The nature and delocalisation of the DSNDI radical within the anionic MOF was further examined using *in situ* X-band EPR spectroelectrochemistry. The initial spectrum at 0 V was characterised by a weak isotropic signal that was attributed to the formation of a photoradical during sample preparation that is characteristic of NDI containing materials.[33,35,36] Upon application of an electrochemical potential the intensity of the signal was observed to increase to give a sharp, isotropic signal (Fig. S6a, ESI†) with a simulated (Fig. S6b, ESI†) g-value of 2.0014, consistent with the formation of an organic radical. The sharpness of the spectrum implied the presence of unresolved hyperfine splitting of the signal. The EPR spectrum of the electrochemical radical at 1.2 V was recollected (Fig. S7, ESI†) using a modulation amplitude of 0.1 G to yield a poorly resolved 13-line spectrum arising from hyperfine splitting of the signal. The latter is consistent with the EPR spectroelectrochemistry from previously reported studies of NDI radical anions that also exhibit a characteristic 13-line signal arising from hyperfine coupling of the NDI radical to the ^{14}N and ^{1}H nuclei of the NDI moiety.[34]
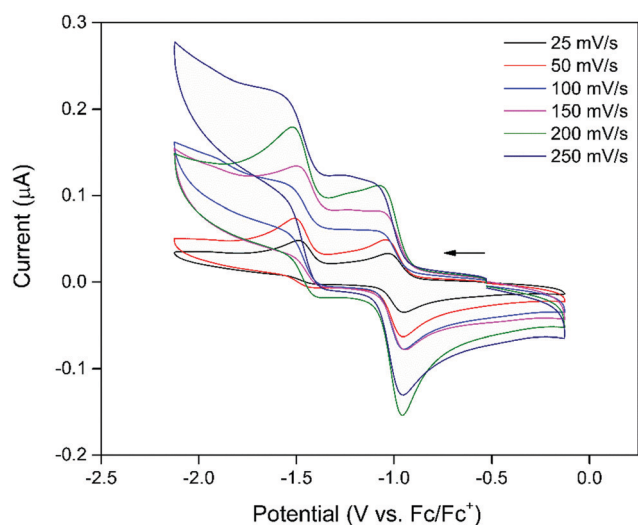
Fig. 2   Solid-state UV-Vis-NIR spectroelectrochemistry of **1** in 0.1 M [(*n*-C$_4$H$_9$)$_4$N]PF$_6$/DMF electrolyte showing potential changes from (a) 0 to −1.2 V and (b) −1.2 to −2.0 V where the arrows indicate the direction of the spectral progression. The step at 12 500 cm^{-1} is due to a detector change. Insets: Photographs of the sample acquired *in situ* during the time-course of the experiment.

Porosity and gas sorption properties

The sorption properties of neutral **1** were examined using N$_2$, H$_2$, CO$_2$ and CH$_4$, extending upon the work of Saha who reported the N$_2$ BET surface area of the material.[26] The DMF solvated *de novo* material was first activated according to a similar procedure to that previously reported.[26] The retention of structure and crystallinity after both solvent exchange and activation was confirmed using capillary PXRD (Fig. S8, ESI†) prior to gas sorption analysis.

The N$_2$ sorption properties at 77 K were characterised by Type IV isotherm behaviour (Fig. 3a) with a minor hysteresis observed in the high pressure region that was suggestive of a microporous structure with a high concentration of vacant adsorption sites. Applying BET theory yielded a surface area of 1748 ± 40 m^2 g^{-1}, a value comparable to those reported for structurally analogous MOF-74 materials,[12,37] but slightly lower than that previously reported for **1** (*cf.* 2044 m^2 g^{-1}) by Saha and co-workers.[26] Although not significantly different, the discrepancy may reflect differences in activation methods between this and

the previous study.[26] Further analysis of the N$_2$ isotherm data enabled the characterisation of the pore size distribution (Fig. S9, ESI†) and pore volume, with a single pore size of 22.5 Å (in good agreement with the 23.8 Å pore width from the calculated model structure) and associated pore volume of 0.53 cm^3 g^{-1} calculated.

Given the strong interest in CO$_2$ capture and storage with respect to MOF-74 materials, the CO$_2$ adsorption properties of **1** were examined at three temperatures of 298, 308 and 318 K (Fig. S10, ESI†). The CO$_2$ isotherms were indicative of Type I sorption behaviour and modest uptake with a maximum of 1.27 mmol g^{-1} of CO$_2$ adsorbed at 1200 mbar and 298 K (Fig. 3b).

Type I behaviour was also observed with respect to the H$_2$ (Fig. S11, ESI†) and CH$_4$ (Fig. S12, ESI†) sorption properties (Table 1) of the MOF, with considerably lower uptake of CH$_4$ observed at 298 K (0.24 mmol g^{-1} at 1200 mbar) relative to CO$_2$. The variance in uptakes of CO$_2$ *vs.* CH$_4$ were tentatively attributed to the differences in binding strength of the respective guests (Fig. S13–S15, ESI†). Previous literature reports have demonstrated
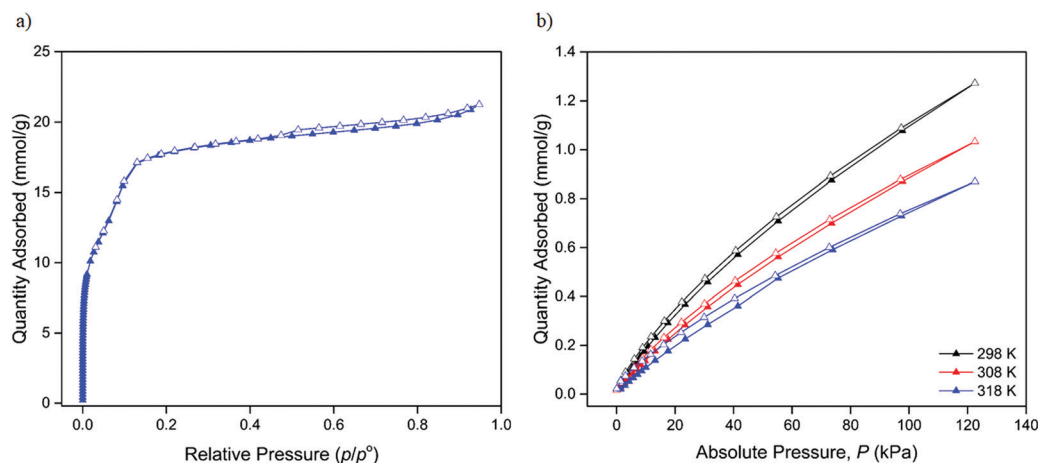

Fig. 3   Gas sorption isotherms of **1** showing adsorption of (a) N$_2$ at 77 K and (b) CO$_2$ at 298, 308 and 318 K. Adsorption and desorption are indicated by closed and open triangles respectively.

Table 1 Sorption properties, H_2 and CO_2 Q_{st} values of **1**. Q_{st} values are reported at the lowest attainable loading

Compound	[Zn₂(DSNDI)]
BET surface area (m² g⁻¹)	1748
Pore volume (cm³ g⁻¹)	0.53
CO₂ 298 K loading (mmol g⁻¹)[a]	1.27
H₂ Q_{st} (kJ mol⁻¹)	7.1
CO₂ Q_{st} (kJ mol⁻¹)	27.5
CH₄ Q_{st} (kJ mol⁻¹)	18.3

[a] 1 bar at 298 K.

a preference of MOF-74 materials to adsorb CO_2 over CH_4 due to its greater polarisability and steric influences that prevent effective binding of the CH_4 molecule at the open metal sites.[38] Conversely, the smaller size and linear geometry of CO_2 facilitate stronger interactions with the open metal sites leading to enhanced uptake relative to CH_4.

Upon completion of the gas sorption experiments the material was examined again using capillary PXRD (Fig. S16, ESI†) to assess the effects of multiple sorption and desorption cycles of guests on the framework stability and structure. PXRD confirmed that the structure had indeed been retained with minimal changes in crystallinity (Fig. S16, ESI†).

Chemical modulation of guest uptake

In order to examine the effects of the electroactivity of the framework on the sorption properties, chemical reduction of the activated material **1** was carried out using 0.1 M lithium naphthalenide (LiNP) in 0.5, 1.0, 2.0, 3.0, 4.0 and 5.0 stoichiometric equivalents to yield chemically reduced MOFs. All reduced samples were washed with dry THF to remove any residual LiNP or naphthalene from the framework post-reduction. The actual degree of framework reduction was determined using ICP-MS, with the measured ratio of Li to Zn used to quantify the extent of reduction (ESI,† Table S3). The reduced frameworks (hereafter denoted by their actual extent of reduction) were found to have retained both structure and crystallinity as confirmed by capillary PXRD (Fig. S17, ESI†). Solid state IR spectroscopy (Fig. S18, ESI†) and TGA (Fig. S34–S40, ESI†) of the reduced samples following the washing procedure also confirmed the removal of residual naphthalene from the pore space.

The solid state UV-Vis-NIR spectra (Fig. 4) of the chemically reduced samples showed distinct changes relative to the neutral material. Highly intense visible bands were observed at 13 070, 14 460, 16 210, 18 480 and 20 530 cm⁻¹ and were attributed to the formation of the DSNDI radical anion.[34] Additional higher energy transitions at 26 840, 31 560, 38 070 and 43 410 cm⁻¹ were also found for these samples. The visible bands were assigned to the formation of the DSNDI radical anion and correlated well with those from the spectroelectrochemical experiment, while the higher energy bands were assigned to the aromatic transitions of the ligand.[33,34] EPR spectroscopy of the reduced samples (Fig. S19–S24, ESI†) also confirmed the successful reduction of the framework with simulated signals (Fig. S25, ESI†) corresponding to the DSNDI radical anion (g = 2.0029) observed.
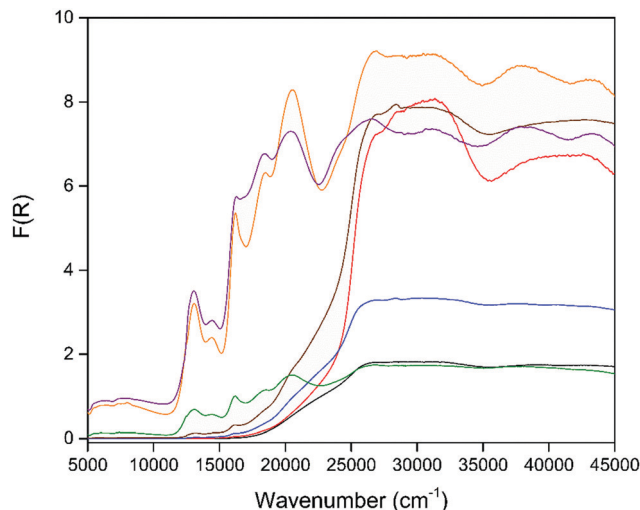

Fig. 4 Solid-state UV/Vis/NIR spectra of [Zn₂(DSNDI)], **1** (black) and its reduced analogues generated by chemical reduction with 0.39 (red), 0.47 (blue), 1.15 (brown), 1.82 (green), 2.27 (orange) and 2.83 equiv. (purple) of LiNP.

The surface areas of the chemically reduced materials were calculated from the N_2 isotherm data at 77 K (Fig. S26, ESI†). Although the N_2 sorption isotherms for the reduced samples showed a qualitative similarity to that of the neutral material, the BET surface areas (Table 2) were found to be considerably lower, with increasing Li loading correlated with lower surface areas. The N_2 uptake was also found to decrease dramatically, with the relatively low uptakes for the 2.27 and 2.82 equiv. samples attributed to the presence of Li^+ counterions, required to charge balance the DSNDI radical anions, within the pore space. Interestingly, although a single pore was detected in the reduced samples, akin to the neutral material, the pore sizes were slightly larger than that of the neutral MOF. This may reflect a possible structural conditioning post-reduction to accommodate the newly introduced DSNDI radical ligands and corresponding Li^+ counterions, as has been observed previously.[31,39] Although not detected, some residual neutral naphthalene may be present in the reduced samples which could be influencing the BET surface areas; however, this contribution cannot be deconvoluted from the relatively larger effect of Li^+ filling the pore space. Future work will focus on the effects of other reducing agents and the effects on CO_2 binding.

The adsorption properties with respect to CO_2 at 298, 308 and 318 K were examined for the samples chemically reduced

Table 2 BET surface areas and pore sizes of the neutral and chemically reduced forms of **1**

Material	BET surface area (m² g⁻¹)	Pore size (Å)
Neutral	1748 ± 40	22.5
0.39 equiv.	1462 ± 100	25
0.47 equiv.	1298 ± 124	24.2
1.15 equiv.	1129 ± 45	24.8
1.82 equiv.	1084 ± 44	24.9
2.27 equiv.	950 ± 79	24.7
2.83 equiv.	889 ± 22	24.8

by 0.39, 0.47, 1.15 and 1.82 equiv. of LiNP. Although still maintaining modest porosity, the CO_2 uptake of the 2.27 and 2.83 equiv. samples were characterised by very low uptakes and extremely long equilibration times. This was attributed to the occlusion of the pore space by Li^+ counterions preventing diffusion and uptake of large, polarisable guests such as CO_2. As such, only the sorption properties of the samples reduced by 0.39, 0.47, 1.15 and 1.82 equiv. are considered here, with all four materials demonstrating Type I sorption behaviour (Fig. 5a and Fig. S27–S29, ESI†). The uptakes of CO_2 were found to be lower than those in the neutral material at all three temperatures, with a maximum uptake of 0.95 mmol g^{-1} recorded for the 0.47 equiv. sample at 298 K, a discrepancy attributed to the occupation of the pore space with Li^+. Given previous reports demonstrating the tuning of the CO_2 binding affinities of porous MOF materials using redox modification,[24,28–30] the CO_2 isosteric heats of adsorption (Q_{st}) of the chemically reduced forms of **1** were of great interest. Applying the Clausius–Clapeyron equation (see ESI†) to the CO_2 isotherms obtained at 298, 308 and 318 K for the 0.39, 0.47, 1.15 and 1.82 equiv. samples yielded Q_{st} profiles (Fig. 5b and Fig. S30, S31, ESI†) for all four samples.

The CO_2 Q_{st} value of the neutral form of **1** was calculated as 27.9 kJ mol^{-1}, a value similar to that of the analogous Zn-MOF-74 analogue (30.6 kJ mol^{-1});[40] this is unsurprising as the chemical environment of the parent system (Zn^{2+} open metal sites and an aromatic ligand system) resembles that of **1** with no major differences expected. The CO_2 Q_{st} values (Table 3) of the 0.39 and 0.47 equiv. samples were similar to that of the neutral material, this being attributed to the relatively low degree of reduction that the framework had undergone. The sample reduced by 1.15 equiv. of LiNP demonstrated a larger increase in its CO_2 binding affinity with a value of 43.9 kJ mol^{-1}, while the sample reduced by 1.82 equiv. had a relatively lower Q_{st} of 22.7 kJ mol^{-1}. It should be noted that the Q_{st} values for the reduced phases were calculated at the lowest pressure data point obtained. Thus, they do not strictly correspond to 'zero-loadings' (*i.e.*, at 0 mbar), where the Q_{st} may be higher.

Table 3 CO_2 298 K loadings and Q_{st} values for the neutral and chemically reduced forms of **1**. Q_{st} values are reported at the lowest attainable loading

Material	CO_2 298 K loading (mmol g^{-1})^a	CO_2 Q_{st} (kJ mol^{-1})
Neutral	1.27	27.9
0.39 equiv.	0.82	25.5
0.47 equiv.	0.95	29.5
1.15 equiv.	0.78	43.9
1.82 equiv.	0.83	22.7

^{a} Bar at 298 K.

The range of CO_2 binding enthalpies recorded for the reduced materials range from weak (25–30 kJ mol^{-1}) to moderately strong (30–50 kJ mol^{-1}) physisorption interactions. Although this trend may suggest that higher Li loadings would lead to higher Q_{st} values, the 1.82 equiv. sample was found to have an enthalpy of adsorption that was approximately half of the maximum value, and 5.2 kJ mol^{-1} lower than that of the neutral MOF. This suggests that a certain 'optimal' Li loading may exist, at which point the CO_2 Q_{st} is maximised, and beyond which the CO_2 binding interactions begin to decrease. While the binding affinities decrease at the higher loadings, the uptakes are still appreciable, suggesting that the high enthalpy sites become self-blocked at high loadings.

The observed modulation of CO_2 binding enthalpies in the chemically reduced frameworks arises due to the changes in the chemical environment due to the formation of organic DSNDI radical anions and the presence of the associated Li^+ counterions. To gain insight into the nature of the host–guest interactions between the framework and the CO_2 and Li^+ guests, DFT calculations (see ESI,† for simulation details) were employed (Fig. S32 and S33, ESI†). The static binding energy of CO_2 in the neutral framework was 31.2 kJ mol^{-1}. For the reduced framework, the initial location of one Li^+ was initially identified from classical simulation, followed by a CO_2 molecule. The latter yielded a binding energy of 55.5 kJ mol^{-1}. The enhanced binding upon reduction is consistent with the experimental observations, and with previously reported examples of redox-modulated framework materials.[28–30,41,42]
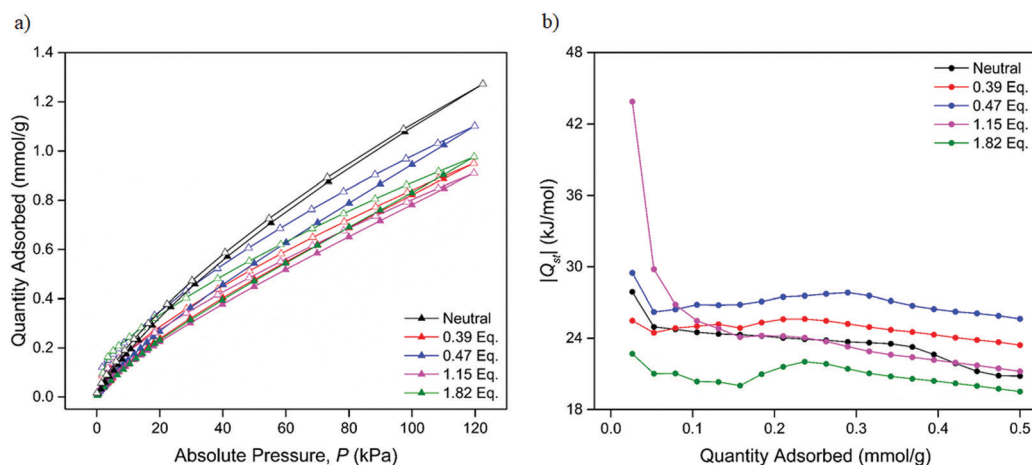

Fig. 5 (a) CO_2 adsorption (closed triangles) and desorption (open triangles) isotherms of the neutral and samples reduced by 0.39, 0.47, 1.15 and 1.82 equiv. of LiNP at 298 K and (b) CO_2 isosteric heat of adsorption profiles for the neutral and chemically reduced samples.

These results demonstrate that the uptake and binding strengths of porous MOF materials can be modified by exploiting the counterion-guest interactions arising from *ex situ* chemical oxidation or reduction.

The successful modulation of the CO_2 Q_{st} values demonstrated a successful proof-of-concept in using chemical reduction as a means to tune the guest affinities of electroactive MOF-74 analogues. Notably, the Q_{st} value of 43.9 kJ mol^{-1} is significantly higher than that of the neutral framework and is comparable to the highest performing member of the MOF-74 series, [$Mg_2(dobdc)$] in terms of its CO_2 binding enthalpy.[3] Given that the present study is concerned only with the Zn^{2+} material, this is both an encouraging result and provides motivation for further study of these electroactive MOF-74 analogues where their intrinsic redox capabilities and open metal binding sites.

Conclusions

A previously reported MOF-74 framework analogue incorporating the redox-active DSNDI ligand has been characterised with a particular focus on its CO_2 sorption and electrochemical properties. The framework was found to successfully retain the electrochemical properties of the discrete DSNDI ligand, exhibiting two reduction processes without loss of electrochemical performance or structural collapse. The BET surface area and CO_2 enthalpy of adsorption were calculated from N_2 and CO_2 adsorption isotherms as 1748 ± 40 m^2 g^{-1} and 27.9 kJ mol^{-1} respectively, values that were comparable to the parent Zn-MOF-74 material. In order to assess the influence of the ligand's electroactive properties on the sorption functionalities of the framework, chemical reduction using LiNP was performed with the resulting materials containing radical DSNDI anionic species as confirmed by both UV-Vis-NIR and EPR spectroscopies. The reduced frameworks also demonstrated structural stability to guest desorption, allowing the gas sorption properties to be assessed. The porosity of the materials was successfully retained despite a decrease in BET surface area that was attributed to the occupation of the pore space by Li^+ counterions. Notably, although the uptake of CO_2 was slightly reduced, a substantial increase in the CO_2 enthalpy of adsorption was observed, with a maximum Q_{st} of 43.9 kJ mol^{-1} obtained for the sample reduced by 1.15 equiv. of LiNP. The enhanced CO_2 Q_{st} value is comparable to the highest performing member of the MOF-74 series, Mg-MOF-74, in terms of its CO_2 binding strength. This strengthening of CO_2 binding from weak to strong physisorption interactions serves as a successful example of the ability to enhance and modulate host–guest affinities by the incorporation of electroactive components into porous framework materials.

Experimental

[$Zn_2(DSNDI)$] framework (1)

The [$Zn_2(DSNDI)$] framework was synthesised according to a previously reported procedure with minor modifications.[26] A screw-cap Pyrex jar was charged with H_4DSNDI (510 mg,

0.95 mmol) and $Zn_2(NO_3)_2 \cdot 6H_2O$ (630 mg, 3.33 mmol) which was suspended and sonicated in a mixture of DMF (90 mL), EtOH (15 mL) and H_2O (15 mL). The mixture was then heated at 90 °C for 24 h before cooling to room temperature, after which the supernatant was decanted and replaced with fresh DMF to remove residual precursors. After soaking for 24 h the target phase was obtained as an orange crystalline powder (0.41 g, 0.61 mmol, 64% based on DSNDI). Elemental Analysis: found: C 47.75%, H 3.81%, N 7.03%; calculated for $C_{28}H_{10}N_2O_{10} \cdot$ 2.5DMF·2H_2O: C 48.24%, H 3.59%, N 7.13%.

Activation of the framework was achieved by exchanging the DMF solvent occupying the pore space with MeOH, with the solvent exchanged twice a day for three days. After heating under dynamic vacuum at 80 °C for 24 h, the activated framework was obtained as a bright yellow crystalline powder. At no point during the soaking or solvent exchanging steps was the sample allowed to go dry or be exposed to air, with the material kept under solvent at all times. The activated material was also protected from exposure to the atmosphere and was handled under an argon atmosphere in a glove box at all times prior to analysis.

Gas sorption analysis

Gas sorption and porosity analysis was performed using a Micromeritics 3-Flex over a 0–1.2 bar pressure range. Approximately 150–200 mg of sample was degassed at 80 °C under vacuum for 18 h prior to measurement. Nitrogen adsorption isotherms were collected at 77 K using an incremental dosing of N_2 gas from 0–1 bar with the Brunauer, Emmett and Teller (BET) model applied to the data to extract the resulting surface area.

H_2 sorption studies were performed at 77 and 87 K while CO_2 and CH_4 sorption was carried out at 298, 308 and 318 K. Isosteric heats of adsorption for H_2, CO_2 and CH_4 were calculated by applying the Clausius–Clapeyron equation to the sorption isotherms obtained at the corresponding temperatures.

Electrochemistry

Electrochemical measurements on solid materials were performed using a BASi Epsilon Electrochemical Analyser. Measurements were recorded using a three electrode set-up consisting of a glassy carbon working electrode, a platinum wire auxiliary electrode and an Ag/Ag$^+$ *quasi*-reference electrode in 0.1 M [(n-C_4H_9)$_4$N]PF$_6$/DMF supporting electrolyte that was degassed with Ar. The sample was mounted by dipping the glassy carbon working electrode into a paste of the powdered sample in DMF. Ferrocene was added at the completion of each experiment as an internal standard with all potentials quoted as V *vs.* Fc/Fc$^+$.

UV-Vis-NIR spectroelectrochemistry

UV-Vis-NIR spectroelectrochemistry of bulk materials was carried out using a CARY5000 spectrophotometer equipped with a Harrick Omni-Diff probe attachment. The Teflon spectroelectrochemical cell consisted of a platinum *quasi*-reference electrode, a silver wire auxiliary electrode and an Indium–Tin–Oxide (ITO) coated glass slide working electrode as reported previously.[43] The sample was immobilised on the

conductive side of the ITO slide using Teflon tape and the applied potential controlled using an eDAQ e-corder 410 potentiostat. 0.1 M $[(n\text{-}C_4H_9)_4N]PF_6/DMF$ supporting electrolyte was used for all measurements with all spectral data reported as the Kubelka–Munk transform, where $F(R) = (1 - R)^2/2R$ (where R is the diffuse reflectance of the sample relative to the Teflon baseline).

Conflicts of interest

The authors declare no conflicts of interest.

Acknowledgements

References

1 K. Sumida, D. L. Rogow, J. A. Mason, T. M. McDonald, E. D. Bloch, Z. R. Herm, T.-H. Bae and J. R. Long, *Chem. Rev.*, 2012, **112**, 724–781.

2 M. Ding, R. W. Flaig, H.-L. Jiang and O. M. Yaghi, *Chem. Soc. Rev.*, 2019, **48**, 2783–2828.

3 A. Das and D. M. D'Alessandro, *CrystEngComm*, 2015, **17**, 706–718.

4 M. I. Gonzalez, M. T. Kapelewski, E. D. Bloch, P. J. Milner, D. A. Reed, M. R. Hudson, J. A. Mason, G. Barin, C. M. Brown and J. R. Long, *J. Am. Chem. Soc.*, 2018, **140**, 3412–3422.

5 J.-R. Li, R. J. Kuppler and H.-C. Zhou, *Chem. Soc. Rev.*, 2009, **38**, 1477–1504.

6 P. Nugent, Y. Belmabkhout, S. D. Burd, A. J. Cairns, R. Luebke, K. Forrest, T. Pham, S. Ma, B. Space, L. Wojtas, M. Eddaoudi and M. J. Zaworotko, *Nature*, 2013, **495**, 80–84.

7 T.-H. Bae and J. R. Long, *Energy Environ. Sci.*, 2013, **6**, 3565–3569.

8 P.-Q. Liao, J.-Q. Shen and J.-P. Zhang, *Coord. Chem. Rev.*, 2018, **373**, 22–48.

9 M. B. Solomon, T. L. Church and D. M. D'Alessandro, *CrystEngComm*, 2017, **19**, 4049–4065.

10 P. M. Usov, B. Huffman, C. C. Epley, M. C. Kessinger, J. Zhu, W. A. Maza and A. J. Morris, *ACS Appl. Mater. Interfaces*, 2017, **9**, 33539–33543.

11 F.-L. Li, Q. Shao, X. Huang and J.-P. Lang, *Angew. Chem., Int. Ed.*, 2018, **57**, 1888–1892.

12 S. R. Caskey, A. G. Wong-Foy and A. J. Matzger, *J. Am. Chem. Soc.*, 2008, **130**, 10870–10871.

13 Y. Liao, L. Zhang, M. H. Weston, W. Morris, J. T. Hupp and O. K. Farha, *Chem. Commun.*, 2017, **53**, 9376–9379.

14 D.-A. Yang, H.-Y. Cho, J. Kim, S.-T. Yang and W.-S. Ahn, *Energy Environ. Sci.*, 2012, **5**, 6465–6473.

15 B. R. Barnett, S. T. Parker, M. V. Paley, M. I. Gonzalez, N. Biggins, J. Oktawiec and J. R. Long, *J. Am. Chem. Soc.*, 2019, **141**, 18325–18333.

16 E. D. Bloch, M. R. Hudson, J. A. Mason, S. Chavan, V. Crocellà, J. D. Howe, K. Lee, A. L. Dzubak, W. L. Queen, J. M. Zadrozny, S. J. Geier, L.-C. Lin, L. Gagliardi, B. Smit, J. B. Neaton, S. Bordiga, C. M. Brown and J. R. Long, *J. Am. Chem. Soc.*, 2014, **136**, 10752–10761.

17 J. E. Bachman, M. T. Kapelewski, D. A. Reed, M. I. Gonzalez and J. R. Long, *J. Am. Chem. Soc.*, 2017, **139**, 15363–15370.

18 W. L. Queen, M. R. Hudson, E. D. Bloch, J. A. Mason, M. I. Gonzalez, J. S. Lee, D. Gygi, J. D. Howe, K. Lee, T. A. Darwish, M. James, V. K. Peterson, S. J. Teat, B. Smit, J. B. Neaton, J. R. Long and C. M. Brown, *Chem. Sci.*, 2014, **5**, 4569–4581.

19 D. M. D'Alessandro, *Chem. Commun.*, 2016, **52**, 8957–8971.

20 I. Mjejri, C. M. Doherty, M. Rubio-Martinez, G. L. Drisko and A. Rougier, *ACS Appl. Mater. Interfaces*, 2017, **9**, 39930–39934.

21 S. Wang, J. Liu, H. Zhao, Z. Guo, H. Xing and Y. Gao, *Inorg. Chem.*, 2018, **57**, 541–544.

22 M.-S. Yao, X.-J. Lv, Z.-H. Fu, W.-H. Li, W.-H. Deng, G.-D. Wu and G. Xu, *Angew. Chem., Int. Ed.*, 2017, **56**, 16510–16514.

23 E. D. Bloch, L. J. Murray, W. L. Queen, S. Chavan, S. N. Maximoff, J. P. Bigi, R. Krishna, V. K. Peterson, F. Grandjean, G. J. Long, B. Smit, S. Bordiga, C. M. Brown and J. R. Long, *J. Am. Chem. Soc.*, 2011, **133**, 14814–14822.

24 A. F. Cozzolino, C. K. Brozek, R. D. Palmer, J. Yano, M. Li and M. Dincă, *J. Am. Chem. Soc.*, 2014, **136**, 3334–3337.

25 L. Sun, T. Miyakai, S. Seki and M. Dincă, *J. Am. Chem. Soc.*, 2013, **135**, 8185–8188.

26 Z. Guo, D. K. Panda, M. A. Gordillo, A. Khatun, H. Wu, W. Zhou and S. Saha, *ACS Appl. Mater. Interfaces*, 2017, **9**, 32413–32417.

27 K. AlKaabi, C. R. Wade and M. Dincă, *Chemistry*, 2016, **1**, 264–272.

28 C. F. Leong, T. B. Faust, P. Turner, P. M. Usov, C. J. Kepert, R. Babarao, A. W. Thornton and D. M. D'Alessandro, *Dalton Trans.*, 2013, **42**, 9831–9839.

29 K. L. Mulfort and J. T. Hupp, *J. Am. Chem. Soc.*, 2007, **129**, 9604–9605.

30 C. Hua, B. Chan, A. Rawal, F. Tuna, D. Collison, J. M. Hook and D. M. D'Alessandro, *J. Mater. Chem. C*, 2016, **4**, 2535–2544.

31 B. A. Johnson, A. Bhunia, H. Fei, S. M. Cohen and S. Ott, *J. Am. Chem. Soc.*, 2018, **140**, 2985–2994.

32 C. F. Leong, B. Chan, T. B. Faust and D. M. D'Alessandro, *Chem. Sci.*, 2014, **5**, 4724–4728.

33 C. F. Leong, B. Chan, T. B. Faust, P. Turner and D. M. D'Alessandro, *Inorg. Chem.*, 2013, **52**, 14246–14252.

34 G. Andric, J. F. Boas, A. M. Bond, G. D. Fallon, K. P. Ghiggino, C. F. Hogan, J. A. Hutchison, M. A.-P. Lee, S. J. Langford, J. R. Pilbrow, G. J. Troup and C. P. Woodward, *Aust. J. Chem.*, 2004, **57**, 1011–1019.

35 H.-L. Zhang, J.-Z. Liao, W. Yang, X.-Y. Wu and C.-Z. Lu, *Dalton Trans.*, 2017, **46**, 4898–4901.

36 A. Mallick, B. Garai, M. A. Addicoat, P. S. Petkov, T. Heine and R. Banerjee, *Chem. Sci.*, 2015, **6**, 1420–1425.

37 D. Gygi, E. D. Bloch, J. A. Mason, M. R. Hudson, M. I. Gonzalez, R. L. Siegelman, T. A. Darwish, W. L. Queen, C. M. Brown and J. R. Long, *Chem. Mater.*, 2016, **28**, 1128–1138.

38 Y. He, W. Zhou, G. Qian and B. Chen, *Chem. Soc. Rev.*, 2014, **43**, 5657–5678.

39 C. R. Wade, M. Li and M. Dincă, *Angew. Chem., Int. Ed.*, 2013, **52**, 13377–13381.

40 D. Yu, A. O. Yazaydin, J. R. Lane, P. D. C. Dietzel and R. Q. Snurr, *Chem. Sci.*, 2013, **4**, 3544–3556.

41 Y. M. Litvinova, Y. M. Gayfulin, K. A. Kovalenko, D. G. Samsonenko, J. van Leusen, I. V. Korolkov, V. P. Fedin and Y. V. Mironov, *Inorg. Chem.*, 2018, **57**, 2072–2084.

42 H. J. Park and M. P. Suh, *Chem. Sci.*, 2013, **4**, 685–690.

43 P. M. Usov, C. Fabian and D. M. D'Alessandro, *Chem. Commun.*, 2012, **48**, 3945–3947.